Hossain, M. S. *et al.* (2015). *Géotechnique* **65**, No. 2, 147–154 [http://dx.doi.org/10.1680/geot.14.T.021]

TECHNICAL NOTE

Effect of spudcan geometry on penetration and extraction resistance in clay

M. S. HOSSAIN*, J. ZHENG* and A. HUSTON*

Spudcan foundations of various geometries are commonly used in the field for supporting offshore oil and gas drilling (jack-up) rigs. This paper investigates the effect of the spudcan and its base geometry on the penetration and extraction resistance in soft normally and lightly overconsolidated clay. A series of centrifuge tests was undertaken on model spudcans of three different geometries typically used in the field. The spudcans were extracted from penetrations of 2·64~3 (area equivalent) diameters and after an operation period of ~19 months. Additional large-deformation finite-element analyses allowed for exploring a range of spudcan base geometries. Corresponding field data were accumulated. The results from this study have confirmed the accuracy of the assumption of a circular conical-based footing and the use of area equivalent diameter for assessing spudcan penetration resistance, as suggested by ISO guidelines 19905-1. Simulation of a flat-based circular plate resulted in 19% higher resistance compared to that of conical-based footings. For spudcans with cutouts and with a peripheral skirt, maximum penetration resistances were, respectively, 14 and 12% lower, and maximum extraction resistances were 20 and 14% lower compared to those for a general spudcan. The corresponding required jack-up leg length was 9 and 7% higher. The effect of peripheral skirt length was shown to be minimal (at least for length relative to spudcan diameter $\leqslant 0{\cdot}42$).

KEYWORDS: bearing capacity; centrifuge modelling; clays; footings/foundations; numerical modelling; offshore engineering

INTRODUCTION

In the offshore oil and gas industry, 'mobile' three-legged jack-up rigs are used widely in performing most offshore drilling in water depths up to around 150 m. The rigs are supported on spudcan foundations of various complicated geometries – with cutouts, quasi-circular and with or without a short skirt around the periphery. For predicting spudcan penetration depth under a given preload, the recently finalised version of ISO guidelines 19905-1 (ISO, 2012; Wong *et al.*, 2012) recommend using a simplified flat- (Skempton method, Skempton, 1951) or conical-based (Houlsby-Martin method, Houlsby & Martin, 2003) circular foundation with area equivalent diameter. This concept is illustrated in Fig. 1. However, no investigation was carried out to confirm the accuracy of this assumption on mobilised penetration and extraction resistance.

This paper reports the results from an investigation through centrifuge model tests and large-deformation finite-element analyses in soft normally and lightly overconsolidated clay. Spudcans of various geometries and sizes commonly used in the field were considered. Corresponding field data were accumulated. The key aim was to assess the influence of spudcan geometry on penetration and extraction resistance profiles.

Manuscript received 12 August 2014; revised manuscript accepted 27 November 2014. Published online ahead of print 3 February 2015. Discussion on this paper closes on 1 July 2015, for further details see p. ii.

* Centre for Offshore Foundation Systems (COFS), The University of Western Australia, Crawley, WA, Australia.

CENTRIFUGE MODELLING

Experimental programme

The experimental programme was carried out at 200***g*** in the beam centrifuge at the University of Western Australia. It has a swinging platform radius of 1·8 m. The platform seats standard rectangular 'strongboxes', which have internal dimensions of 650 (length) × 390 (width) × 325 (depth) mm, representing a prototype test bed of 130 (long) × 78 (wide) × 65 (deep) m at 200***g***. In total, three spudcan penetration–extraction tests were performed (Table 1). A free water layer was maintained above the test sample.

Tests were performed using three model spudcans (spudcans A, B and C), with full details of the geometry shown in Fig. 2. The shape of spudcan A (Fig. 2(a)) was simplified (following Purwana *et al.*, 2005) from the spudcans of the 'Keppel-Fels, Class B' jack-up rig, as illustrated by Quah *et al.* (2010). In the field, skirted spudcans are sometimes used for various reasons, such as increasing horizontal and moment capacity (InSafeJIP, 2010). To mimic that geometry, a skirt of height 8 mm was added around the periphery of spudcan B (Fig. 2(b)). The shape of spudcan C (Fig. 2(c)) can be taken as similar to the spudcans of the current 116C design, as illustrated by Menzies & Roper (2008). A shaft of $0{\cdot}243D_{eq}$ diameter was used to connect the spudcan to the load actuator.

Preparation of sample

A homogeneous slurry was prepared by mixing commercially available kaolin powder with water and consolidated directly in the centrifuge at 200***g***. To achieve non-homogeneous clay with a non-zero strength intercept at the surface ($s_{um} \neq 0$), the upper 2 mm layer was carefully

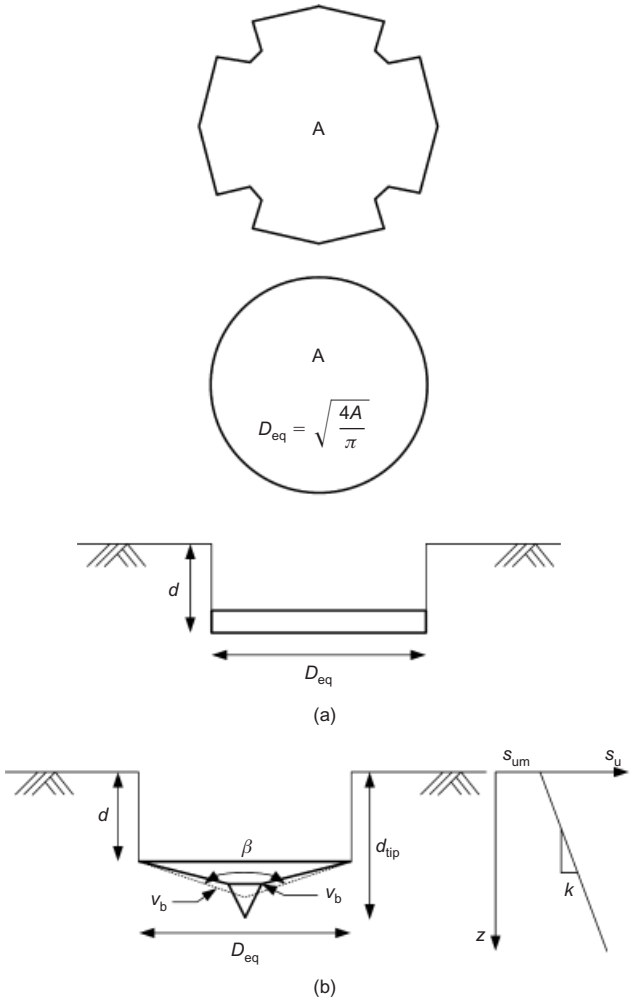

Fig. 1. Simplified equivalent spudcans (following ISO, 2012): (a) flat-based circular plate; (b) conical-based circular footing

trimmed off the consolidated sample. The final sample depth was 250 mm. The spudcans (tip) were penetrated up to 180 mm ($2{\cdot}64{\sim}3D_{eq}$) and hence the bottom boundary was more than one diameter away. To avoid the influence from the bottom boundary, the distance of the footing tip should be $> 0{\cdot}7{\sim}1D_{eq}$ (Mandel & Salencon, 1969; Meyerhof & Hanna, 1978; Ullah *et al.*, 2014).

Test procedure

The process of each test consisted of three stages: installation, operation and extraction of spudcan. The installation of the spudcan was carried out in-flight until the spudcan reached the target depth of $2{\cdot}64{\sim}3$ times spudcan (area equivalent) diameter. The operation period of the spudcan commenced after reducing the installation load (maximum penetration resistance, Q_{in}) on the spudcan by 25% to an operational working load. The operation stage was simulated by maintaining a constant vertical load on the spudcan for a duration of 20 min (~19 months in prototype). Extraction of the spudcan was then performed.

Tests were carried out using a displacement-controlled system, except at the operation stage, when it was swapped to a load-controlled system. The T-bar and spudcans were penetrated–extracted at a rate of 1 mm/s and 0·188 mm/s, respectively, chosen to balance rate effects against ensuring undrained behaviour in the clay. The normalised velocity index $V = vD_{eq}/c_v$ was around 140 (as recommended to ensure undrained behaviour by Chung *et al.* (2006) and Low *et al.* (2008)). It was necessary to ensure undrained behaviour to be consistent with the field installation and extraction of spudcans in clay.

Soil strength determination

Characterisation tests were carried out in-flight using a T-bar penetrometer 5 mm in diameter and 20 mm in length (model scale). Typical undrained shear strength profiles are

Table 1. Summary of centrifuge tests conducted

	This study			Cassidy *et al.* (2009)	
Spudcan	A	B	C	C	D
Test	CA1	CB1	CC1	CC2	CD1
Geometry Diameter (model), D: mm Skirt length (model), L: mm	Spudcan 60 –	Spudcan with skirt 60 8	Spudcan with cutouts 73·2 –	Spudcan with cutouts 73·2 –	Spudcan 72·72 –
Test ***g***-level	200			250	
Diameter (prototype), D: m Area equivalent diameter (prototype), D_{eq}: m Volume equivalent base cone angle, β_{eq}: ° Skirt length (prototype), L: m Spudcan tip height: m Installation depth, d_{tip}	12 12 149·78 – 2·35 $3D_{eq}$	12 12 153·18 1·6 2·5 $3D_{eq}$	14·64 13·65 146·29 – 3·05 $2{\cdot}64D_{eq}$	18·3 17·06 146·29 – 3·81 $0{\cdot}8D_{eq}$	18·18 18·18 146·11 – 2·52 $0{\cdot}63D_{eq}$
Installation strength, $s_{u,p}$: kPa	$0{\cdot}9 + 1{\cdot}95z$			$7{\cdot}5 + 1{\cdot}85z$	
Extraction strength, $s_{u,e}$: kPa	$0{\cdot}5 + 1{\cdot}6z$			$6 + 1{\cdot}4z$	
Soil effective unit weight, γ': kN/m^3	7·5			~7·8	
Sensitivity of soil, S_t	2·91				
Maximum installation resistance, $q_{u,in}$: kPa Breakout force, $q_{u,br}$: kPa	560·38 413·53	491·41 353·73	483·65 330·17	289·47 151·76	307·8 120·13

Fig. 2. Model spudcans: (a) spudcan A: Keppel-Fels, Class B spudcan; (b) spudcan B: skirted spudcan; (c) spudcan C: 116C spudcan; (d) spudcan D: Mod V 'A' Class spudcan (all dimensions in mm)

shown in Fig. 3, based on a T-bar factor of $N_{T\text{-}bar} = 10{\cdot}5$. This type of clay strength profile is prevalent in the Gulf of Mexico ($s_{u,p} = 2{\sim}18 + 1{\sim}2{\cdot}1z$ kPa; Menzies & Roper, 2008; Menzies & Lopez, 2011). An identical bearing factor was used for penetration ($s_{u,p}$) and extraction ($s_{u,e}$), which can be justified from Low *et al.* (2008, 2010). Table 1 presents a summary of idealised $s_{u,p}$ and $s_{u,e}$, effective unit weight γ', and the sensitivity of the soil S_t.

Centrifuge test data from previous study

Cassidy *et al.* (2009) carried out centrifuge tests on 1:250 scale model spudcans of the current 116C and Mod V design (referred to as spudcan C and D, respectively; see Figs 2(c) and 2(d)). Penetration and immediate extraction tests were performed in kaolin clay deposit with $s_{u,p} = 7{\cdot}5 + 1{\cdot}85z$ kPa and $s_{u,e} = 6 + 1{\cdot}4z$ kPa. The details are included in Table 1.

NUMERICAL MODELLING

Three-dimensional (3D) large-deformation finite-element (LDFE) analyses were performed using the coupled Eulerian–Lagrangian (CEL) approach in the commercial finite-element package Abaqus/Explicit (DSS, 2010). The details of numerical implementation of the CEL approach in Abaqus can be found in Qiu & Henke (2011), Qiu & Grabe (2012) and Hossain *et al.* (2014). Only a quarter sector of the soil domain was represented in the analyses, accounting for the inherent symmetry. The spudcan was modelled as a rigid body, which would have an insignificant effect on the overall accuracy of the presented results as spudcan foundations (made of steel) are much stiffer compared to clay deposits and hence deform minimally during penetration. The soil–spudcan interface was modelled as partially rough. The soil domain and spudcan foundation were discretised using hexahedral elements of type EC3D8R and 3D continuum elements of types C3D8R and C3D6, respectively. The penetration velocity of the spudcan in the numerical analysis was taken as 0·1 m/s. The sensitivity analyses showed that this velocity induces minimal inertial effect. This is consistent with the conclusions drawn by Qiu & Henke (2011), Tho *et al.* (2012) and Zheng *et al.* (2014), who adopted a penetration velocity of 0·5 m/s, 0·17 m/s and 0·1 m/s, respectively.

The soil was modelled as a linear elastic–perfectly plastic material obeying a Tresca yield criterion, but extended as described later to capture strain-rate and strain-softening effects. A uniform stiffness ratio of $E/s_u = 500$ (where E is the Young's modulus) was taken throughout the clay profile. All the analyses simulated undrained conditions and adopted a Poisson ratio $\nu = 0{\cdot}49$ and friction and dilation angles $\phi = \psi = 0$ in total stress analysis. The geostatic stress conditions were modelled using $K_0 = 1$, as the stable penetration resistance (once backflow is fully established) has been found to be unaffected by the value of K_0 (Zhou & Randolph, 2009).

Following the proposed model of Einav & Randolph (2005), the Tresca soil model was extended in order to take the combined effects of rate dependency and gradual softening into account. The undrained shear strength at individual Gauss points was modified at the beginning of each time step, according to the average rate of maximum shear strain in the previous increments and the current accumulated absolute plastic shear strain, expressed as

$$s_{uc} = \left[1 + \mu \log\left(\frac{\mathrm{Max}(|\dot{\xi}|, \dot{\xi}_{ref})}{\dot{\xi}_{ref}}\right)\right][\delta_{rem} + (1 - \delta_{rem})\,e^{-3\xi/\xi_{95}}]\,s_u \quad (1)$$

The first bracketed term augments the strength according to the maximum strain rate, $\dot{\xi}$, relative to a reference value, $\dot{\xi}_{ref}$, which was considered as 1·5%/h as consistent with triaxial tests (Lunne *et al.*, 2006), following a logarithmic law with rate parameter μ taken as 0·1 for 'circular' spudcan foundations (Low *et al.*, 2008). The second part of Equation 1 models the degradation of strength according to an exponential function of cumulative shear strain, ξ, from the intact condition to a fully remoulded ratio, δ_{rem} ($= 1/S_t = \alpha$). The relative ductility is controlled by the parameter, ξ_{95}, which represents the cumulative shear strain required for 95% remoulding. A typical value of $\xi_{95} = 15$ (i.e. 1500% shear strain; Randolph, 2004) was considered. Further details can be found in Hossain *et al.* (2014).

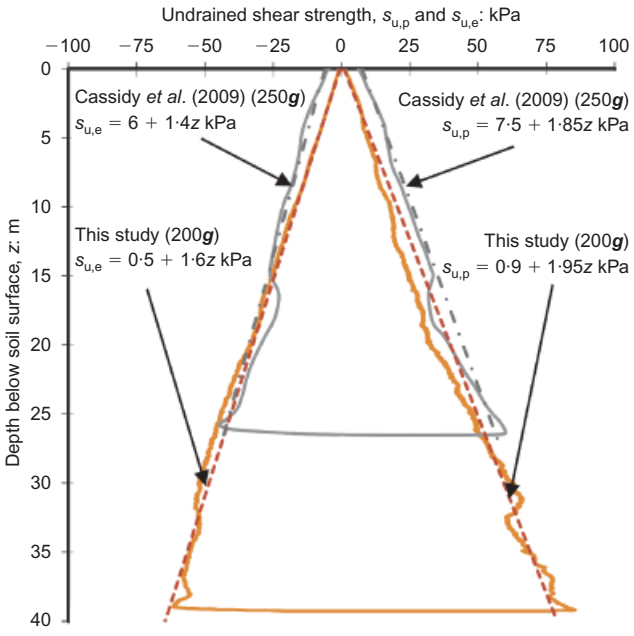

Fig. 3. Undrained shear strength profile from T-bar tests ($N_{T\text{-}bar} = 10{\cdot}5$; '−ve' indicates extraction)

RESULTS AND DISCUSSION

The results are presented in terms of penetration–extraction resistance, Q_p and Q_e, or corresponding normalised resistance, $q_{u,p}$ and $q_{u,e}$, as a function of penetration depth of spudcan tip, d_{tip}, or skirt tip, d_{Ltip}, or normalised depth of spudcan base, d/D_{eq}.

Penetration and extraction resistance: centrifuge tests

Figure 4 shows the results from all penetration–extraction tests (CA1, CB1 and CC1) carried out in this study. Consistent with practice, the results are primarily plotted in resistance Q–d_{tip} space (Fig. 4(a)). At final embedment depth of $d_{tip} = {\sim}35{\cdot}7$ m, maximum installation resistance, Q_{in}, for spudcans C and B is ∼13% higher and ∼7% lower, and maximum extraction resistance (or breakout force), Q_{br}, is ∼3% higher and ∼10% lower compared to those for spudcan A. As D_{eq} of spudcan C is around 1·13 times greater than that of spudcans A and B, the resistance axis in Fig. 4(b) was normalised by spudcan area as $q_u = Q/A$. For spudcan C, $q_{u,in}$ and $q_{u,br}$ are, respectively, 14 and 20% lower, and for spudcan B, they are 12 and 14% lower, respectively. For a typical preload of 400 kPa, the required jack-up leg length is seen to be 9 and 7% higher (see Fig. 4(b)). This difference is evident for depth $d_{tip} > 20$ m, where

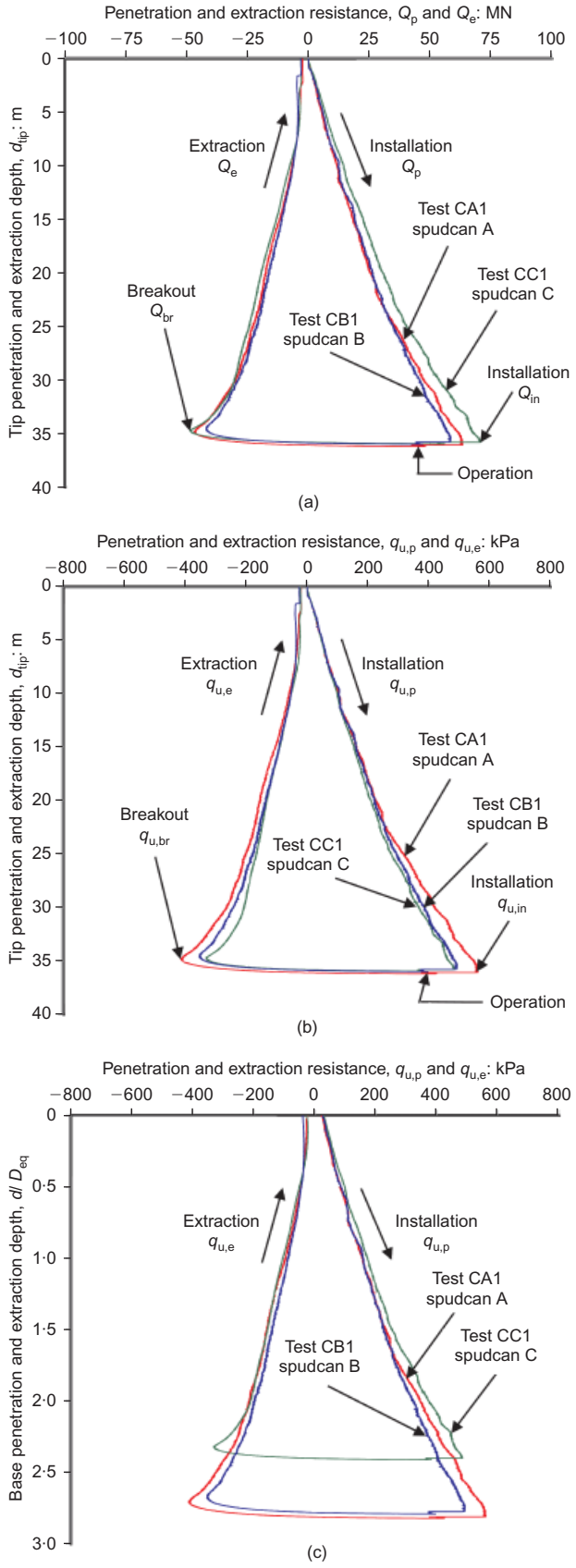

Fig. 4. Penetration and extraction resistance from centrifuge tests (tests CA1, CB1 and CC1; Table 1): (a) Q–d_{tip} space; (b) q_u–d_{tip} space; (c) q_u–d/D_{eq} space

a fully localised, deep flow-round soil failure mechanism prevailed (Hossain *et al.*, 2014). At this stage, the lower normalised penetration resistance or higher leg penetration for spudcan C is due to shorter flow path through the cutouts (less energy required), and for spudcan B is attributed to the fact that softer soil from the surface was trapped at the base of the advancing spudcan inside the skirt. Fig. 4(c) shows the results as a function of d/D_{eq} to be consistent with the general bearing capacity calculation, which is performed in relation to the depth of spudcan base level, d.

Figure 5 shows the resistance profiles from tests on spudcans C and D reported by Cassidy *et al.* (2009). For this shallow penetration depth of $d_{tip} < 12{\cdot}7$ m, the results are consistent on q_u–d_{tip} space.

Penetration resistance: LDFE analyses

To explore the effect of simplification of spudcan base geometry following the ISO approaches, as illustrated in Fig. 1, LDFE analyses were carried out simulating the penetration of spudcan A, equivalent conical-based circular footing and flat-based circular plate (NA1, NA2, NA3; Table 2). The soil undrained shear strength was considered as identical to the centrifuge test of this study (see Table 2), with the other properties noted in the previous section on 'Numerical modelling'. The results are displayed in Fig. 6. In both Q_p–d_{tip} and Q_p–d/D_{eq} spaces, penetration of the foundations with conical-based geometries (with or without a spigot) resulted in consistent resistance profiles due to mobilisation of similar soil failure mechanisms, with trapping of similar degree of softer soil at the base of the foundations at any penetration depth. By contrast, penetration of the flat-based circular plate resulted in remarkably higher resistance (e.g. 19% at $d/D_{eq} = 2$ on Q_p–d/D_{eq} space; Fig. 6(b)) partly due to more vertically downward flow (i.e. through soil of higher resistance for this soil with strength increasing with depth) and partly due to trapping less softer soil at the base of the foundations at any penetration depth. Penetration of the sloping bottom (and top) of a conical-based footing causes less shearing of the adjacent soil. Increasing penetration resistance with increasing cone angle β is consistent with lower bound solutions reported by Houlsby & Martin (2003).

To demonstrate the effect of skirt length, LDFE analyses were also performed varying $L = 1{\cdot}6$ m (identical to spudcan B), 2·5 m (equal to the tip height of spudcan B) and 5 m ($>$ the tip height of spudcan B) (NB1, NB2, NB3; Table 2). Again, the soil undrained shear strength was identical to the centrifuge test of this study (see Table 2). The penetration resistance profiles are displayed in Fig. 7 as a function of

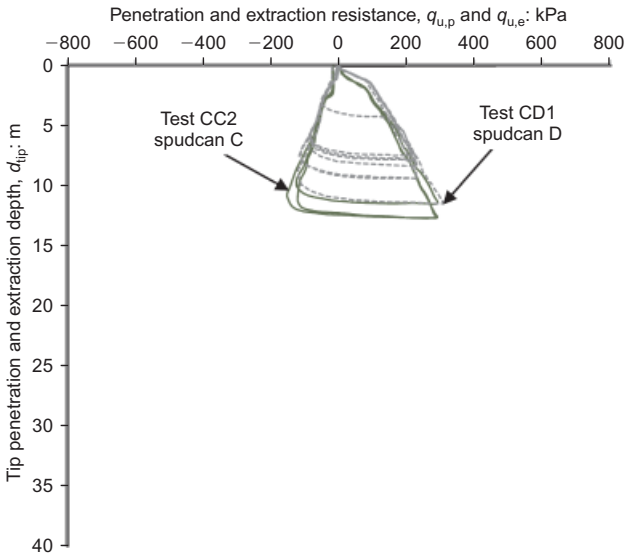

Fig. 5. Penetration and extraction resistance from centrifuge tests (tests CC2 and CD1; Table 1)

Table 2. Summary of LDFE analyses conducted

Spudcan	A			B		
Analysis	NA1	NA2	NA3	NB1	NB2	NB3
Geometry	Spudcan	Flat-based circular plate	Conical-based circular footing	Spudcan with skirt		
Diameter, D: m	12	12	12	12	12	12
Area equivalent diameter, D_{eq}: m	12	12	12	12	12	12
Volume equivalent base cone angle, β_{eq}: °	149·78	180	149·78	153·18	153·18	153·18
Skirt length, L: m	–	–	–	1·6	2·5	5
Spudcan tip height: m	2·35	0	1·62	2·5	2·5	2·5
$s_{u,p}$: kPa	0·9 + 1·95z	0·9 + 1·95z	0·9 + 1·95z	0·9 + 1·95z	0·9 + 1·95z	0·9 + 1·95z

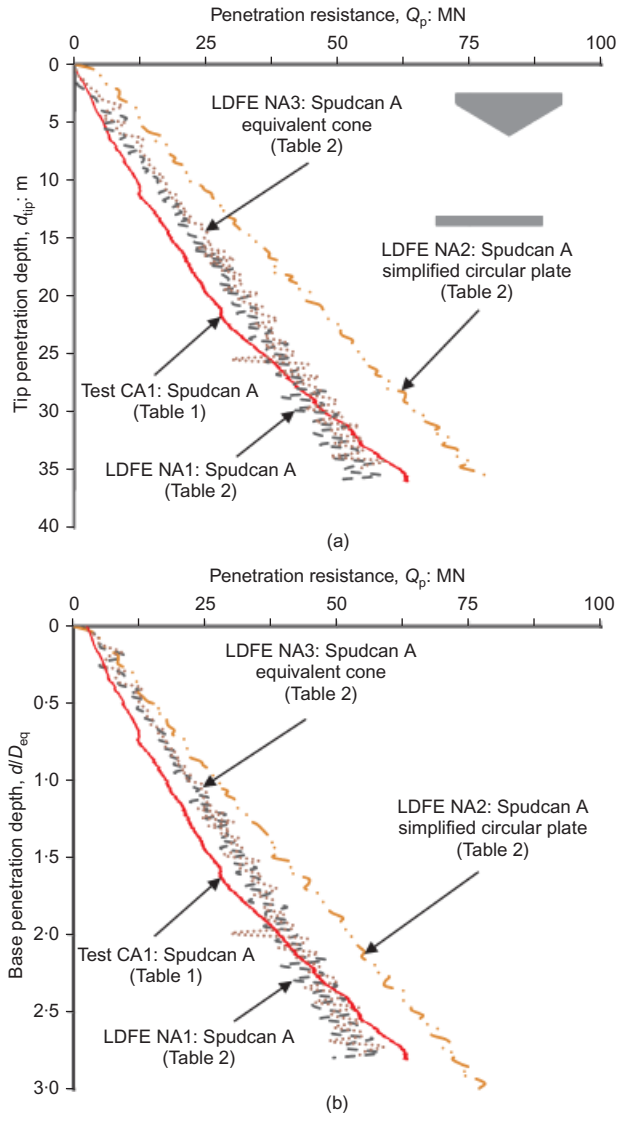

Fig. 6. Effect of spudcan base geometry on penetration resistance (NA1, NA2, NA3; Table 2): (a) Q_p–d_{tip} space; (b) Q_p–d/D_{eq} space

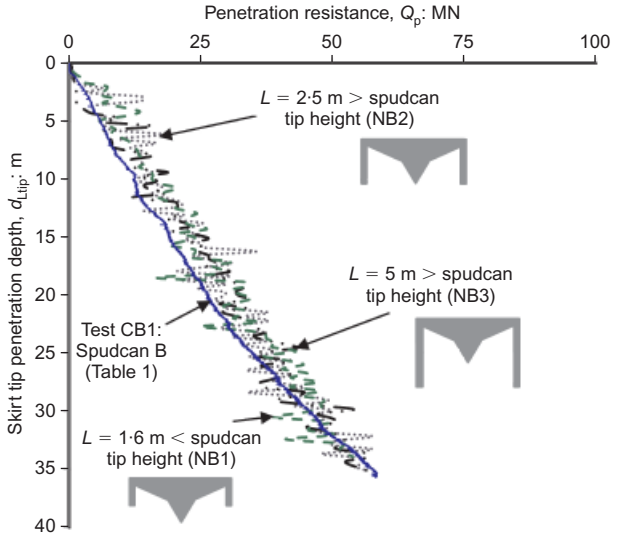

Fig. 7. Effect of skirt length, L, on penetration resistance (NB1, NB2, NB3; Table 2)

penetration depth of skirt tip assuming that the effective spudcan base was shifted to the skirt tip level after trapping of softer material inside the skirt. The effect of increasing L is counterbalanced by the increasing amount of trapped softer soil inside the skirt, leading to negligible resultant influence.

Hossain *et al.* (2014) used the same numerical model and performed analyses for several case histories (discussed in the following subsection 'Penetration resistance: field data') for simulating actual spudcan geometries with cutouts as well as idealised circular spudcans with (area) equivalent diameter, D_{eq}. The results indicate minimal effect of this idealisation; an example is shown in Fig. 8.

The corresponding results from centrifuge tests CA1 and test CB1 are also included in Figs 6 and 7, respectively, showing good agreement with the computed profiles. In addition, Fig. 8 shows excellent agreement with field data. This confirms the accuracy of the numerical model used.

Penetration resistance: field data

Menzies & Roper (2008) and Hossain *et al.* (2014) reported case histories from 14 different locations in the Gulf of Mexico. The soils were predominantly normally and lightly overconsolidated clay with undrained shear strength increasing with depth. Full details of the soil profiles and spudcan geometries were given by Menzies & Roper (2008) and Hossain *et al.* (2014). Nine different types of spudcan geometry were used for the selected case histories. Based on this study, the spudcans can be categorised as: (a) spudcan (sites 1~9 and sites 12~14); (b) flat-based circular plate (site 10); and (c) conical-based circular footing (site 11). The spudcan equivalent diameters vary from 10·6 to 16·3 m. For unifying the data, measured penetration resistance was normalised by the corresponding spudcan area and local undrained shear strength at the spudcan base level, giving bearing capacity factor, $N_c = Q_p/A/s_{u0}$. Fig. 9 shows the

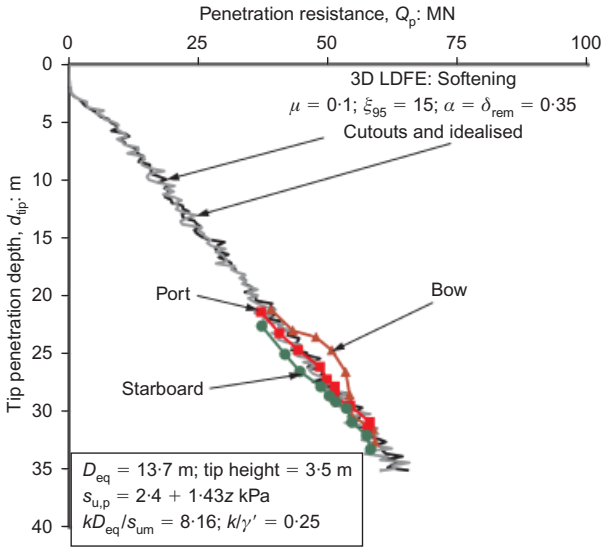

Fig. 8. Effect of cutout or equivalent spudcan diameter (data reported by Hossain *et al.*, 2014)

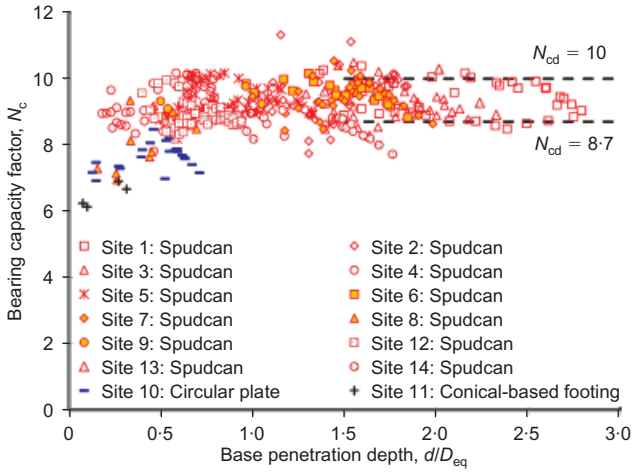

Fig. 9. Effect of spudcan base geometry on bearing capacity factor (field data reported by Menzies & Roper (2008) and Hossain *et al.* (2014))

factors from 14 sites as a function of d/D_{eq}, indicating no clear evidence of a remarkable influence of spudcan geometry, apart from the effect of shallow and transitional failure mechanisms for various soil strength non-homogeneity (kD_{eq}/s_{um}) at shallow penetration depths ($d/D_{eq} < \sim 1$). The values of bearing capacity factor at deep penetrations can be bracketed by two dashed lines representing $N_{cd} = 8{\cdot}7$ and 10 (see Fig. 9).

CONCLUDING REMARKS

The experimental and numerical work reported in this paper explored the effect of spudcan and its base geometry and idealisation following ISO guidelines 19905-1. The comparative results have confirmed the following.

(*a*) For spudcans with cutouts and with a peripheral skirt, maximum penetration resistances were, respectively, 14 and 12% lower, and maximum extraction resistances were 20 and 14% lower compared to those for a general spudcan. The corresponding required jack-up leg lengths were 9 and 7% higher.

(*b*) The effect of peripheral skirt length was shown to be minimal (at least for length relative to spudcan diameter $\leqslant 0{\cdot}42$).

(*c*) For design, the use of equivalent circular footing, equivalent conical-based, and area equivalent diameter, as suggested by ISO guidelines 19905-1, was shown to be reasonable.

(*d*) However, the use of an equivalent flat-based circular plate resulted in 19% higher resistance compared to that of conical-based footings.

(*e*) For spudcans of various geometries, penetration resistance at deep penetrations can be assessed using $N_{cd} = 8{\cdot}7 \sim 10$ with local undrained shear strength at the spudcan base level.

ACKNOWLEDGEMENTS

The first author is an ARC Discovery Early Career Researcher Award (DECRA) Fellow and is supported by the ARC Project DE140100903. The work forms part of the activities of the Centre for Offshore Foundation Systems (COFS), currently supported as a node of the Australian Research Council Centre of Excellence for Geotechnical Science and Engineering and as a Centre of Excellence by the Lloyd's Register Foundation. This support is gratefully acknowledged, as is the assistance of the beam centrifuge technician, Mr Manuel Palacios.

NOTATION

A	plan area of spudcan at largest section or outer base area of skirted foundation
c_v	coefficient of consolidation
D	diameter of spudcan at largest section or outer diameter of skirted foundation
D_{eq}	(plan area) equivalent diameter of spudcan
d	depth of spudcan base (lowest point of largest section)
d_{Ltip}	penetration depth of skirt tip
d_{tip}	penetration depth of spudcan tip
E	Young's modulus
K_0	at-rest earth pressure coefficient
k	rate of increase of undrained shear strength with depth
L	length of skirt
N_c	bearing capacity factor of spudcan
N_{cd}	deep bearing capacity factor of spudcan
$N_{T\text{-}bar}$	bearing capacity factor of T-bar penetrometer
Q	penetration–extraction resistance
Q_{br}	maximum extraction resistance
Q_e	extraction resistance
Q_{in}	maximum penetration resistance
Q_p	penetration resistance
q_u	normalised penetration–extraction resistance
$q_{u,br}$	maximum normalised extraction resistance
$q_{u,e}$	normalised extraction resistance
$q_{u,in}$	maximum normalised penetration resistance
$q_{u,p}$	normalised penetration resistance
S_t	soil sensitivity
s_u	intact undrained shear strength of clay
s_{uc}	current undrained shear strength after considering softening and rate effect
$s_{u,e}$	undrained shear strength of clay during extraction
$s_{u,p}$	intact undrained shear strength of clay during penetration
s_{um}	intact undrained shear strength at mudline (i.e. $z = 0$)
s_{u0}	intact undrained shear strength at spudcan base level, d
V	normalised velocity index
v	penetration rate of object
z	depth below soil surface
α	spudcan–soil interface friction ratio (base roughness)
γ'	effective unit weight of soil
δ_{rem}	remoulded ratio (inverse of sensitivity)
μ	rate parameter
ν	Poisson's ratio
ξ	absolute cumulative plastic shear strain
ξ_{95}	softening parameter

$\dot{\xi}$ maximum shear strain rate
$\dot{\xi}_{ref}$ reference shear strain rate at which s_u was assessed
ϕ friction angle
ψ dilation angle

REFERENCES

Cassidy, M. J., Quah, C. K. & Foo, K. S. (2009). Experimental investigation of the reinstallation of spudcan footings close to existing footprints. *J. Geotech. Geoenviron. Engng, ASCE* **135**, No. 4, 474–486.

Chung, S. F., Randolph, M. F. & Schneider, J. A. (2006). Effect of penetration rate on penetrometer resistance in clay. *J. Geotech. Geoenviron. Engng, ASCE* **132**, No. 9, 1188–1196.

DSS (Dassault Systèmes Simula Corp.) (2010). *Abaqus 6·10 online documentation*. Providence, RI, USA: Dassault Systèmes Simula Corp.

Einav, I. & Randolph, M. F. (2005). Combining upper bound and strain path methods for evaluating penetration resistance. *Int. J. Numer. Methods Engng* **63**, No. 14, 1991–2016.

Hossain, M. S., Zheng, J., Menzies, D., Meyer, L. & Randolph, M. F. (2014). Spudcan penetration analysis for case histories in clay. *J. Geotech. Geoenviron. Engng, ASCE* **140**, No. 7, 04014034-1–04014034-13.

Houlsby, G. T. & Martin, C. M. (2003). Undrained bearing capacity factors for conical footings on clay. *Géotechnique* **53**, No. 5, 513–520, http://dx.doi.org/10.1680/geot.2003.53.5.513.

InSafeJIP (2010). *Improved guidelines for the prediction of geotechnical performance of spudcan foundations during installation and removal of jack-up units*, Joint Industry Funded Project. Abingdon, UK: RPS Energy.

ISO (2012). ISO 199051-1: Petroleum and natural gas industries – Site specific assessment of mobile offshore units – Part 1: Jack-ups. Geneva, Switzerland: International Organization for Standardization.

Low, H. E., Randolph, M. F., DeJong, J. T. & Yafrate, N. J. (2008). Variable rate full-flow penetration tests in intact and remoulded soil. *Proceedings of the 3rd international conference on geotechnical and geophysical site characterization*, pp. 1087–1092. Taipei, Taiwan: Taylor & Francis Group.

Low, H. E., Lunne, T., Andersen, K. H., Sjursen, M. A., Li, X. & Randolph, M. F. (2010). Estimation of intact and remoulded undrained shear strengths from penetration tests in soft clays. *Géotechnique* **60**, No. 11, 843–859, http://dx.doi.org/10.1680/geot.9.P.017.

Lunne, T., Berre, T., Andersen, K. H., Strandvik, S. & Sjursen, M. (2006). Effects of sample disturbance and consolidation procedures on measured shear strength of soft marine Norwegian clays. *Can. Geotech. J.* **43**, No. 7, 726–750.

Mandel, J. & Salencon, J. (1969). The bearing capacity of soils on a rock foundation. *Proceedings of the 7th international conference on soil mechanics and foundation engineering*, pp. 157–164. Mexico City, Mexico: Sociedad Mexicana de Mecanica.

Menzies, D. & Lopez, C. R. (2011). Four atypical jack-up rig foundation case histories. *Proceedings of the 13th international conference on the jack-up platform: design, construction and operation*, London.

Menzies, D. & Roper, R. (2008). Comparison of jackup rig spudcan penetration methods in clay. *Proceedings of the offshore technology conference*, Houston, TX, paper OTC 19545.

Meyerhof, G. G. & Hanna, A. M. (1978). Ultimate bearing capacity of foundations on layered soils under inclined load. *Can. Geotech. J.* **15**, No. 4, 565–572.

Purwana, O. A., Leung, C. F., Chow, Y. K. & Foo, K. S. (2005). Influence of base suction on extraction of jack-up spudcans. *Géotechnique* **55**, No. 10, 741–753, http://dx.doi.org/10.1680/geot.2005.55.10.741.

Qiu, G. & Grabe, J. (2012). Numerical investigation of bearing capacity due to spudcan penetration in sand overlying clay. *Can. Geotech. J.* **49**, No. 12, 1393–1407.

Qiu, G. & Henke, S. (2011). Controlled installation of spudcan foundations on loose sand overlying weak clay. *Mar. Structs* **24**, No. 4, 528–550.

Quah, C. K., Cahyadi, J., Purwana, O. A., Krisdani, H. & Randolph, M. F. (2010). An integrated system for improving geotechnical performance of jack-up rig installation. *Proceedings of the Asia Pacific drilling technology conference and exhibition*, Ho Chi Minh City, IADC/SPE 135970. Richardson, TX, USA: Society of Petroleum Engineers.

Randolph, M. F. (2004). Characterisation of soft sediments for offshore applications. Keynote lecture. *Proceedings of the 2nd international conference on site characterisation*, Porto, vol. 1, pp. 209–231. Rotterdam, the Netherlands: Millpress.

Skempton, A. W. (1951). The bearing capacity of clays. *Proceedings of the building research congress*, London, vol. 1, pp. 180–189.

Tho, K. K., Leung, C. F., Chow, Y. K. & Swaddiwudhipong, S. (2012). Eulerian finite-element technique for analysis of jack-up spudcan penetration. *Int. J. Geomech*. **12**, No. 1, 64–73.

Ullah, S. N., Hu, Y., White, D. & Stanier, S. (2014). LDFE study of bottom boundary effect in foundation model tests. *Int. J. Phys. Modelling Geotech*. **14**, No. 3, 80–87.

Wong, P. C., Templeton, III. J. S., Purwana, O. A., Hofstede, H., Cassidy, M. J., Hossain, M. S. & Martin, C. M. (2012). Foundation modeling and assessment in the new ISO standard 19905-1. *Proceedings of the offshore technology conference*, Houston, TX, paper OTC 23521.

Zheng, J., Hossain, M. S. & Wang, D. (2014). Numerical modelling of spudcan deep penetration in three-layer clays. *Int. J. Geomech*. http://dx.doi.org/10.1061/(ASCE)GM.1943–5622.0000439.

Zhou, H. & Randolph, M. F. (2009). Resistance of full-flow penetrometers in rate-dependent and strain-softening clay. *Géotechnique* **59**, No. 2, 79–86, http://dx.doi.org/10.1680/geot.2007.00164.